Available online at www.sciencedirect.com
ScienceDirect
Metamaterials 5 (2011) 26–35
Metamaterials
www.elsevier.com/locate/metmat

Invited Paper

In-plane modal analysis of a metalayer formed by arrayed pairs of dogbone-shaped conductors

P. Baccarelli [a,*], F. Capolino [b], S. Paulotto [a], A.B. Yakovlev [c]

[a] *Department of Information Engineering, Electronics and Telecommunications, Sapienza University of Rome, Via Eudossiana 18, 00184 Rome, Italy*
[b] *Department of Electrical Engineering and Computer Science, University of California, Irvine, CA 92697, USA*
[c] *Department of Electrical Engineering, University of Mississippi, MS 38677-1848, USA*

Received 6 December 2010; received in revised form 2 February 2011; accepted 4 February 2011
Available online 13 February 2011

Abstract

We present a comprehensive analysis of natural modes of a planar metamaterial layer (metalayer) formed by arrayed pairs of metallic dogbone-shaped conductors separated by a thin dielectric layer. The in-plane modes are classified based on the symmetric and anti-symmetric current distributions in the pairs. Of particular interest are the anti-symmetric modes, since the anti-symmetric current is associated with the magnetic resonance in metamaterial particles made of tightly coupled pairs. It is shown that the modal spectrum includes both TE and TM bound (proper real) and leaky (proper complex and improper complex) modes. An interesting observation is that a peculiar dominant TM improper leaky wave with a low attenuation constant, for the anti-symmetric current distribution, occurs at low frequencies, with a potential application in periodic leaky-wave antennas.

PACS: 41.20.Jb (electromagnetic wave propagation; radiowave propagation)

Keywords: Planar metamaterial layer; Surface waves; Leaky waves; Backward waves; Stopbands

1. Introduction

Backward waves through a metamaterial made of a stack of layers (metalayers) formed by arrayed pairs of dogbone-shaped conductors separated by an electrically thin dielectric layer, have been recently analyzed [1]. The design proposed in [1], based on electromagnetically tightly coupled paired scatterers (in the sense of electromagnetic interaction, without electrically connecting the paired conductors), constitutes indeed a general strategy in the realization of bulk [three-dimensional (3D)] metamaterials [2]. The pairing approach has been used in a variety of examples, from microwaves [3–5] to optical frequencies [6,7]. Recently, dogbone-like particles have been extended to the two-dimensional (2D) isotropic case by using pairs of metallic Jerusalem crosses [8,9] and pairs of tripoles [10]. In contrast to metamaterials made of split-ring resonators and wires, the designs proposed in [1,8] are fully planar, which is advantageous when few layers are needed, especially at very high frequencies, e.g., millimeter-wave and THz frequencies. In [1], the authors have focused on analyzing the symmetric and anti-symmetric mode resonances supported by each pair in the constitutive cells, and on the nega-

* Corresponding author. Tel.: +39 06 44585452; fax: +39 06 44585918.
E-mail addresses: baccarelli@die.uniroma1.it (P. Baccarelli), f.capolino@uci.edu (F. Capolino), yakovlev@olemiss.edu (A.B. Yakovlev).

1873-1988/$ – see front matter © 2011 Elsevier B.V. All rights reserved.
doi:10.1016/j.metmat.2011.02.002

tive refraction index behavior for waves traveling across stacked layers. It has been shown that a metamaterial made by stacking layers of dogbone pairs supports a positive-index frequency band at low frequencies, and a negative-index frequency band at slightly higher frequencies.

In most of the studies on metamaterials, researchers have limited their analyses to the plane-wave incidence orthogonal to the metamaterial layers. Metamaterials proposed in the past may guide waves along different directions, especially in the presence of anisotropy. However, even a single metamaterial layer (metalayer) and, in general, a stack of planar layers may support modal propagation in the planar direction (along the metalayers), which could significantly alter the metamaterial performance. Indeed, localized scatterers, imperfections, or transverse truncation of layers would be capable of exciting modes propagating along the metalayer. The intention of this work is to shed light on unusual guided propagation along metalayers, with particular attention to in-plane modes with anti-symmetric current distributions. Moreover, peculiar features of this kind of metamaterial arrangement, such as the transmission and reflection properties through a layer of dogbone pairs, can find a suitable alternative or complementary explanation in terms of the relevant in-plane modal characteristics [11]. In addition, the presence of appropriate leaky modes of the metalayer is potentially useful in the design of leaky-wave antennas, when a proper excitation is considered.

In this work, the modal (wavenumber–frequency) dispersion in the planar direction for a single metalayer made of pairs of dogbone-shaped metallic conductors is analyzed by using a well-established method of moments approach [12], whose results have been validated for a variety of planar periodic structures with different *ad hoc* and commercial full-wave software [12–14]. Surface waves (i.e., bound waves) and proper and improper leaky waves are accurately investigated for a metalayer. The natural modes are classified in terms of TE and TM polarizations of the symmetric dielectric slab, which are perturbed by the presence of arrayed pairs of metallic dogbones, and in this paper will be referred to as perturbed TE and TM modes. Furthermore, these modes are categorized in terms of their symmetric or anti-symmetric current distributions with respect to the symmetry plane between the two conductors, at $z = 0$ in Fig. 1.

In previous studies one of the co-authors has shown that anti-symmetric currents exhibit a resonance (called "magnetic resonance"), which is related to artificial magnetism and thus responsible for the negative refractive index in a metalayer made by a stack of dogbone layers [1,2]. Here, we clearly show that such anti-symmetric current distribution can be associated, in a certain frequency range, with a TM improper leaky wave propagating along the metalayer, which can give rise to leaky-wave radiation in proximity of the magnetic resonance when excited by a localized source. Furthermore, it can be noted that, because of the image principle, an anti-symmetric current distribution in a layer of thickness H of dogbone pairs is equivalent to a current distribution in a layer of single dogbones at a distance $H/2$ from a ground plane. Therefore, our analysis is directly applicable to the study of modal propagation in artificial magnetic surfaces (as high-impedance surfaces). Indeed, such a structure (i.e., a single layer of dogbones or, more generally, Jerusalem crosses, printed on a thin grounded dielectric slab) has been used as an artificial magnetic substrate [15,16] for a low-profile dipole antenna [17,18].

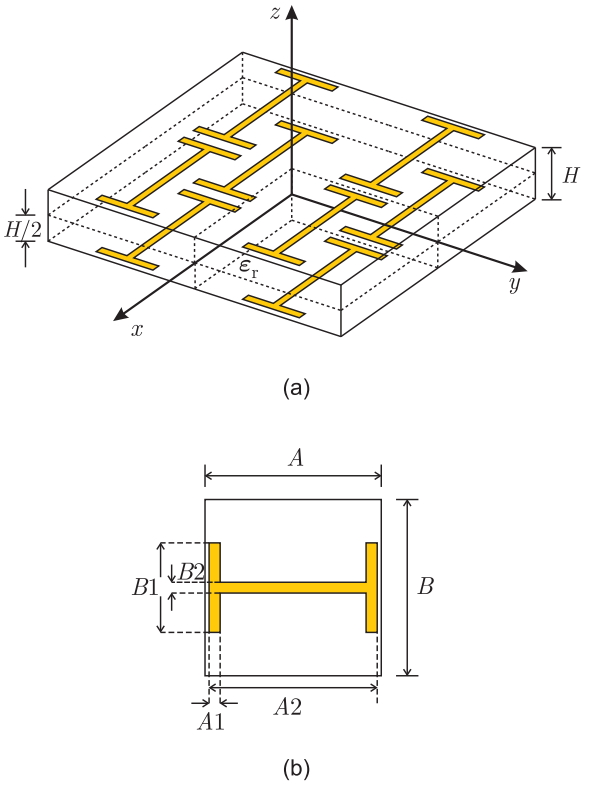

Fig. 1. (a) A layer of the metamaterial formed by a periodic arrangement, along x- and y-directions, of tightly coupled pairs of dogbones. (b) Top view of the metamaterial unit cell, periodic along the x- and y-directions, with periods A and B, respectively. In all simulations the following default parameters have been used: $A = B = 7.5$ mm, $A_1 = B_2 = 0.5$ mm, $A_2 = 7.4$ mm, and $B_1 = 4$ mm. The substrate has thickness $H = 2$ mm and dielectric constant $\varepsilon_r = 2.2$, as in [8].

The paper is organized as follows. A summary of Floquet representation for periodic structures is given in Section 2, followed in Section 3 by the analysis of dispersion properties of symmetric and anti-symmetric in-plane natural modes for a layer of electromagnetically tightly coupled pairs of dogbones. Conclusions are drawn in Section 4.

2. Modal analysis – Floquet representation

A complete characterization of modal spectrum is proposed for the metalayer with the geometry shown in Fig. 1. Since the structure consists of a dielectric layer with a 2D array of dogbone pairs in the x–y plane, symmetric with respect to the plane $z=0$, the analysis has been carried out in terms of symmetric and anti-symmetric modes. A modal propagation along the principal transverse directions (x and y) is considered. Because of the periodicity (with spatial periods A and B along x and y, respectively), modal fields admit the following representation

$$\mathbf{E}(x,\ y,\ z) = \sum_{m,n=-\infty}^{+\infty} \mathbf{e}_{mn}(z) e^{-jk_{x,m}x} e^{-jk_{y,n}y} \tag{1}$$

in terms of an infinite number of Floquet harmonics along the x- and y-directions, with complex propagation wavenumbers [12,19],

$$k_{x,m} = \beta_{x,m} - j\alpha_x = \left(\beta_{x,0} + \frac{2\pi m}{A}\right) - j\alpha_x \tag{2}$$

$$k_{y,n} = \beta_{y,n} - j\alpha_y = \left(\beta_{y,0} + \frac{2\pi n}{B}\right) - j\alpha_y \tag{3}$$

The time dependence $e^{j\omega t}$ is assumed and suppressed. It should be noted that we assume without loss of generality $(m,n)=(0,0)$ for the fundamental harmonic. Away from the planes $z=H/2$ and $z=-H/2$, the Floquet harmonics of a mode behave as $\mathbf{e}_{mn}(z) \propto \exp(-jk_{z,mn}|z|)$, where the z-directed (m,n)th Floquet wavenumber is

$$k_{z,mn} = \sqrt{k_0^2 - k_{x,m}^2 - k_{y,n}^2} = \beta_{z,mn} - j\alpha_{z,mn} \tag{4}$$

and k_0 is the free-space wavenumber. Depending on the value of the phase and attenuation constants in the x- and y-directions, we distinguish among a few cases categorized in [12,19]. Surface-wave modes bounded to the layer do not radiate power away from the transverse plane containing the periodic structure, i.e., *all* Floquet harmonics have a phase velocity slower than that of light in the surrounding medium, i.e., $\left(\beta_{x,m}^2 + \beta_{y,n}^2\right)^{1/2} > k_0$, for all (m,n) indexes. Vice versa, *physical* leaky modes are the complex modes that radiate power away from the transverse plane containing the periodic structure, because *at least one* Floquet harmonic has a phase velocity faster than that of light in the surrounding medium, i.e., $\left(\beta_{x,m}^2 + \beta_{y,n}^2\right)^{1/2} < k_0$, for at least one pair of (m,n). We observe [see (2) and (3)] that all Floquet wavenumbers $k_{x,m}$ and $k_{y,n}$, with varying indexes m and n, have the same imaginary parts α_x and α_y, respectively. Based on the choice of the imaginary part of the vertical wavenumber of the Floquet harmonics $k_{z,mn}$, different cases are distinguished based on $\alpha_{z,mn}>0$ (proper, or exponentially decaying for increasing $|z|$) and $\alpha_{z,mn}<0$ (improper, or exponentially growing for increasing $|z|$) [12,19]. A leaky mode with one or more improper Floquet harmonics can be physical, as detailed in [12]. However, a more general definition of physical and non-physical modes is related to an excitation problem, such that a physical mode is a mode that can be excited by a source, whereas a non-physical mode is a mathematical solution and cannot be excited [19–21]. A thorough description of leaky modes can be found in [22–26].

We finally recall that in the lossless case, the mathematical modal solution $(k_{x,m}, k_{y,n})$ of the transcendental equation, for structures that satisfy the reciprocity theorem like the present one, exhibit certain symmetry properties. In particular, if $k_{x,m}$ is a solution, when $k_{y,0}=0$ and $n=0$, then, due to the conjugate property of the modal solution and to the bidirectionality property of the periodic structure [28,29], there are other three modal solutions [30]: $-k_{x,m}$, $(k_{x,m})^*$, and $(-k_{x,m})^*$, where the asterisk * means complex conjugate. Whereas, for a lossy case only one symmetry property is satisfied, i.e., if $k_{x,m}$ is a solution, then $-k_{x,m}$ is also a solution [29].

3. Symmetric and anti-symmetric modes

The in-plane natural modes, in the array of dogbone pairs, are classified in terms of their symmetry with respect to the plane $z=0$, which is the geometrical symmetry plane (Fig. 1). The modes with currents flowing on the metallic dogbone pairs in the same direction, for $z>0$ and $z<0$, are defined as symmetric modes. Vice versa, the modes with currents flowing in the opposite directions, for $z>0$ and $z<0$, are denoted as anti-symmetric modes [1,2]. We took advantage of this classification based on the symmetry by modeling a half of the structure in the presence of either a perfect electric conductor (PEC) or perfect magnetic conductor (PMC) symmetry plane placed in the middle of the layer. Therefore, numerically we model only the top conductor on half of the dielectric layer with either PEC or PMC plane, and

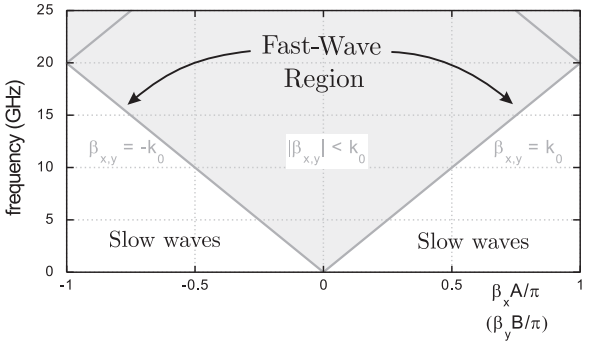

Fig. 2. Brillouin diagram showing the radiative (fast-wave) and bound (slow-wave) regions for modes propagating along the principal axes for the 2D periodic structure as in Fig. 1(a). The lines $\beta_{x,y} = \pm k_0$ and their periodic replicas are plotted using gray solid lines. The fast-wave region is indicated as a shadowed gray region.

periodic boundary conditions imposed along the x- and y-directions.

Because of space limitation, and without deterring the quality of the information, we show here only complex modes with the fundamental $(m, n) = (0, 0)$ harmonic propagating along the principal axes, i.e., either $k_{y,0} = 0$ (modes propagating along the x-direction) or $k_{x,0} = 0$ (modes propagating along the y-direction). In particular, the complete dispersion properties of phase constants $\beta_{x,m}$ and $\beta_{y,n}$ of Floquet harmonics propagating along the principal x- and y-directions, respectively, are presented by using the Brillouin dispersion diagram shown in Fig. 2, where bound, stopband, and radiating regimes can be easily displayed [25]. The dispersive behavior of the Floquet harmonics is reported as a plot of frequency versus $\beta_x A/\pi$ ($\beta_y B/\pi$) in the first Brillouin zone, i.e., $-1 < \beta_x A/\pi < 1$ ($-1 < \beta_y B/\pi < 1$) in Fig. 2, where β_x (β_y) represents the phase constant of any particular Floquet harmonic along x- (or y-) direction, and A (B) is the period [25,31].

It should be noted that, for modes propagating along the x- (or y-) direction, a fast Floquet harmonic is such that $|\beta_{x,m}| < k_0$ ($|\beta_{y,n}| < k_0$) and, hence, it lies in the shadowed gray region (fast-wave region) in the Brillouin diagram in Fig. 2. Furthermore, a fast Floquet harmonic is leaky forward (improper determination) if $\beta_{x,m}\alpha_x > 0$ ($\beta_{y,n}\alpha_y > 0$), which implies that the leaky mode is attenuated along the positive or negative x- (or y-) direction, i.e., $\alpha_x > 0$ ($\alpha_y > 0$) or $\alpha_x < 0$ ($\alpha_y < 0$), respectively, and the Floquet harmonic radiates in free space with $\beta_{x,m} > 0$ ($\beta_{y,n} > 0$) or $\beta_{x,m} < 0$ ($\beta_{y,n} < 0$), respectively [12,19,25]. In contrast, a fast Floquet harmonic is leaky backward (proper determination) if $\beta_{x,m}\alpha_x < 0$ ($\beta_{y,n}\alpha_y < 0$), which implies that the leaky mode is attenuated along the positive or negative x- (or y-) direction, i.e., $\alpha_x > 0$ ($\alpha_y > 0$) or $\alpha_x < 0$ ($\alpha_y < 0$), respectively, and the Floquet harmonic radiates in free space with $\beta_{x,m} < 0$ ($\beta_{y,n} < 0$) or $\beta_{x,m} > 0$ ($\beta_{y,n} > 0$), respectively [12,19,25]. A physical leaky mode has at least one proper or improper Floquet harmonic which is in the fast-wave region in Fig. 2.

In the following, we will observe and classify in-plane modes with both positive and negative group velocities $\partial\omega/\partial\beta_{x,m}$ (or $\partial\omega/\partial\beta_{y,n}$) in the first Brillouin zone. In general, a forward Floquet harmonic has phase and group velocities along the same direction and is displayed in the Brillouin diagram with a dispersion curve that has a positive (negative) slope when the phase constant is positive (negative), whereas a backward Floquet harmonic has phase and group velocities along opposite directions and is displayed in the Brillouin diagram with a dispersion curve that has a negative (positive) slope when the phase constant is positive (negative) [25,31].

Since the dogbones are mainly sensitive to the electric field polarized along the direction of the dogbone central conductor (the x-direction in Fig. 1), modes with the electric field mainly polarized along the y-direction will behave similar to those in a dielectric slab of thickness H (without dogbones). In contrast, the modes with the electric field along the x-direction are strongly affected by the presence of the dogbones.

In this paper we have chosen the dimensions of dogbones and the periodicities of dogbone pairs along x and y as in [8], so that the in-plane modal analysis presented here can be associated with the metamaterial performance shown in [8]. It should be noted that in [8] an array of pairs of Jerusalem crosses was analyzed, which however behaves as an array of dogbone pairs for a fixed polarization with electric field along one of the axes. Therefore, the default chosen parameters as defined in Fig. 1 are: $A = B = 7.5$ mm, $A_1 = B_2 = 0.5$ mm, $A_2 = 7.4$ mm, and $B_1 = 4$ mm. The substrate has thickness $H = 2$ mm and dielectric constant $\varepsilon_r = 2.2$, as in [8].

3.1. Symmetric modes: TE and TM polarizations

3.1.1. Modes propagating along the x-direction

The TE modes of a dielectric slab with thickness H propagating along x (i.e., the modes with the electric field mainly along the y-direction) are weakly perturbed by the dogbone conductors at low frequencies. In Fig. 3(a) the normalized Floquet-harmonic phase constants $\beta_{x,m}A/\pi$ of the fundamental perturbed TE_0 mode (gray curves) are shown as function of frequency in the first Brillouin region ($-1 < \beta_x A/\pi < 1$) of the Brillouin diagram. At low frequencies this mode, which does not have cutoff, behaves similar to that of the dielectric slab with

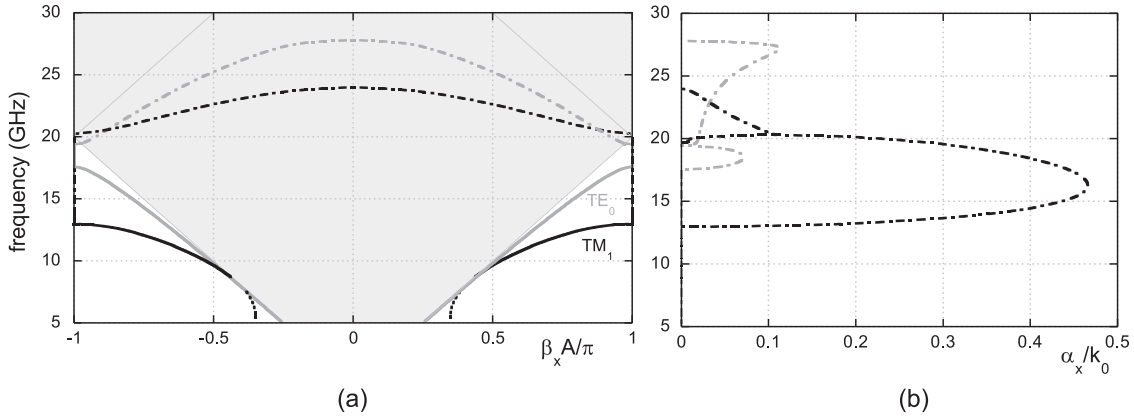

Fig. 3. Brillouin diagram: (a) frequency versus normalized phase constant $\beta_x A/\pi$ and (b) frequency versus normalized attenuation constant α_x/k_0 for symmetric modes propagating along the x-direction. Legend: (a) *phase constant*: solid lines – proper real; dashed-dotted lines – proper complex; dotted lines – improper real. (b) *Attenuation constant*: dashed-dotted lines – proper complex. The lines $\beta_x = \pm k_0$ are reported as light gray solid lines. The fast-wave region is indicated as a shadowed gray region.

the phase constant of the fundamental $(m, n) = (0, 0)$ harmonic (gray solid curve) that is almost superimposed to the light line $\beta_x = \pm k_0$ (light gray thin solid lines in Fig. 3(a)). When the frequency increases the TE_0 mode interacts with the dogbone pairs and in the frequency range between 17.5 GHz and 19.5 GHz it is in a closed stopband regime (associated with the Bragg diffraction condition, i.e., the period is equal to a half of the guided wavelength of this mode), and becomes a proper complex mode (gray dashed-dotted lines), as can be seen from the values of the normalized attenuation constant α_x/k_0 shown in Fig. 3(b). [Since we are considering all the four valid solutions at a given frequency, i.e., $k_{x,m}$, $-k_{x,m}$, $(k_{x,m})^*$, and $(-k_{x,m})^*$, positive and negative values of the normalized attenuation constant should be shown in Fig. 3. However, for sake of readability we show only the values $\alpha_x > 0$.] At the highest edge of the closed stopband region this mode turns into a proper leaky wave $(m, n) = (-1, 0)$ Floquet harmonic as gray dashed-dotted line in Fig. 3(a)), which becomes physical in the fast-wave region $-1 < \beta_x/k_0 < 1$, indicated as a shadowed gray region in Fig. 3(a). In particular, when observing along the $+x$-direction ($\alpha_x > 0$), the $(m, n) = (-1, 0)$ Floquet harmonic is physical when $-1 < \beta_x/k_0 < 0$, and vice versa, when observing along the $-x$-direction ($\alpha_x < 0$), it is physical when $0 < \beta_x/k_0 < 1$. In both cases $\beta_{x,-1}\alpha_x < 0$, which confirms the proper (backward) nature of the physical leaky wave. We can also observe that this kind of leaky wave is characterized by phase and group velocities that are in opposite directions, i.e., the dispersion curves in the shadowed gray region in Fig. 3(a) have a negative (positive) slope when the phase constant is positive (negative), and can give rise to radiation of the backward type when the leakage constant shown in Fig. 3(b) is sufficiently low, as in the present case.

Also in Fig. 3, the dispersion behavior of perturbed TM_1 symmetric mode propagating along x (the magnetic field is mainly along y) is shown (black curves). The TM polarization is strongly affected by the x-aligned dogbones. It should be noted that the cutoff of the perturbed TM_1 mode is approximately 8 GHz, while that in the corresponding dielectric slab without dogbones is equal to 69 GHz. The perturbed TM_1 mode experiences a large bandgap between 13 GHz and 20 GHz with high values of the attenuation constant. At higher frequency this mode turns into a backward leaky wave (the $(m, n) = (-1, 0)$ Floquet harmonic indicated as black dashed-dotted curves in Fig. 3(a)), which is physical within the fast-wave region (shadowed gray region in Fig. 3(a)) and can radiate in free space.

A pure real improper solution arises below the cutoff frequency of the perturbed TM_1 mode (black dotted curves in Fig. 3(a)) which is a non-physical solution. No improper leaky waves are present at low frequencies. At higher frequencies, when both the phase and attenuation constants of the perturbed TM_1 and TE_0 leaky waves become equal to zero (at 24 GHz and 27.75 GHz, respectively), transitions to improper leaky waves occur that are followed by open stopband regimes [31] with strong attenuation (not reported in Fig. 3).

A complete bandgap region for propagation along the x-direction in the case of PMC symmetry is observable between 17.5 GHz and 19.5 GHz.

3.1.2. Modes propagating along the y-direction

The TE modes, polarized along x, greatly couple with the dogbone structure when propagating along the

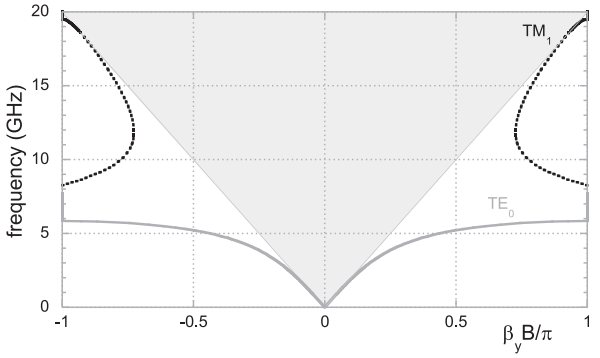

Fig. 4. Symmetric modes propagating along the y-direction. Brillouin diagram (frequency versus $\beta_y B/\pi$). Legend: solid lines – proper real; dotted lines – improper real. The lines $\beta_y = \pm k_0$ are reported as light gray solid lines. The fast-wave region is indicated as a shadowed gray region.

y-direction. In Fig. 4 the phase constant of the fundamental $(m, n) = (0, 0)$ harmonic of the perturbed TE_0 mode is shown in the first Brillouin zone $-1 < \beta_y B/\pi < 1$. A strong perturbation is visible at low frequencies, which leads to a wide bandgap for this mode (characterized by very high values of the attenuation constant, not reported here) for frequencies above 5.8 GHz; below this frequency the mode is in a surface-wave regime (gray solid lines). As concerns the TM_1 mode $(m, n) = (0, 0)$ harmonic as black curves in Fig. 4], it is weakly perturbed and it exists as surface wave between its cutoff frequency (approximately 18.6 GHz) and 19.5 GHz, above which the mode is in a stopband regime. Below the cutoff frequency, it continues as a non-physical real improper solution (black dotted curve).

For propagation along the y-direction, proper and improper leaky waves with low attenuation constants are absent. Furthermore, a wide complete bandgap region is observable between 5.8 GHz and 18.6 GHz, as it is shown in Fig. 4.

3.2. Anti-symmetric modes: TE and TM polarizations

3.2.1. Modes propagating along the x-direction

The perturbed anti-symmetric TE modes in the array of pairs of dogbones (the modes with the electric field polarized mainly along the y-direction) are similar to the anti-symmetric TE modes in a dielectric slab with thickness H because the electric field interacts weakly with the dogbone pairs (directed along x) at low frequencies. As a consequence, a proper real surface-wave behavior for the perturbed anti-symmetric TE_1 mode does not exist, since in a dielectric slab with thickness H the TE_1 cutoff frequency is above 19.96 GHz (which corresponds to the tip of the light-line triangle in the Brillouin diagram in Fig. 5(a), i.e., the higher-frequency limit for the bound region), and, therefore, it is completely suppressed.

The dispersion behavior of anti-symmetric perturbed TM modes (magnetic field mainly along the y-direction) of arrays of dogbone pairs is shown in Fig. 5. As it can be noted from the Brillouin diagram in Fig. 5(a), a perturbed TM_0 mode is present, which propagates as a proper real forward mode below 10 GHz in its passband regime $(m, n) = (0, 0)$ harmonic as black solid curves in Fig. 5(a)). The perturbed TM_0 mode is in a stopband regime between 10 GHz and 17.96 GHz with the typical behavior of the attenuation constant in this

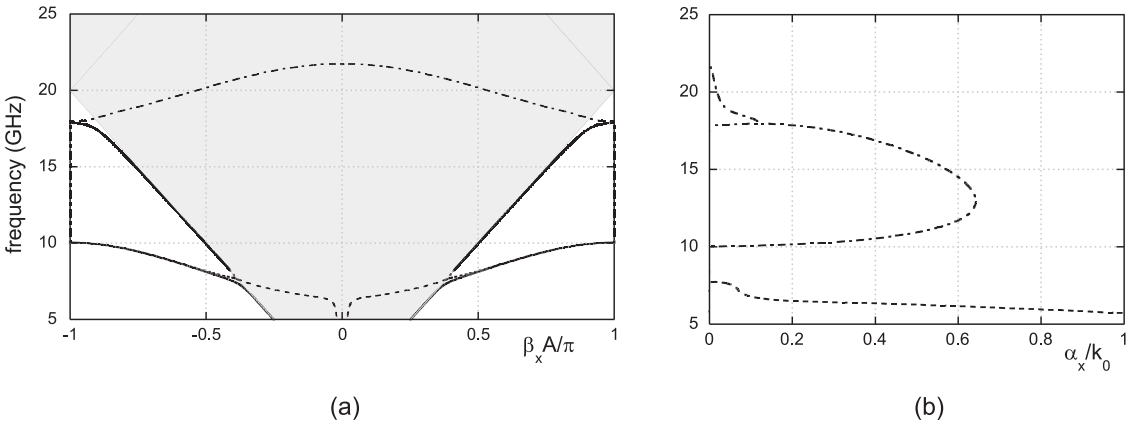

Fig. 5. Anti-symmetric TM modes propagating along the x-direction. Brillouin diagram: (a) frequency versus normalized phase constant $\beta_x A/\pi$ and (b) frequency versus normalized attenuation constant α_x/k_0 for the structure in Fig. 1. Legend: (a) *phase constant*: solid lines – proper real; dashed-dotted lines – proper complex; dotted lines – improper real; dashed lines – improper complex. (b) *Attenuation constant*: dashed-dotted lines – proper complex; dashed lines – improper complex. The curves $\beta_x = \pm k_0$ are reported as light gray solid lines. The fast-wave region is indicated as a shadowed gray region.

regime (black dashed-dotted line in Fig. 5(b)). Above 17.96 GHz it exits from the stopband region as a proper leaky wave $(m,n)=(-1,0)$ Floquet harmonic as black dashed-dotted line in Fig. 5(a)) with low values of the attenuation constant. By further increasing frequency, the $(m,n)=(-1,0)$ Floquet harmonic becomes fast and lies in the fast-wave region $-1<\beta_x/k_0<1$, indicated as a shadowed gray region in Fig. 5(a), between 18.2 GHz and 21.7 GHz, where it can give rise to radiation of the backward type. At approximately 21.7 GHz both the phase and attenuation constants of the TM_0 proper leaky wave become equal to zero and a transition to an improper leaky wave occurs, followed by an open stopband [31] with high values of the attenuation constant (not shown here).

A second proper real branch of the perturbed TM_0 mode is present between 8.25 GHz and 17.85 GHz $(m,n)=(0,0)$ harmonic as black solid curves in Fig. 5(a)); at low frequencies it is weakly perturbed and almost superimposed to the light line (gray dashed lines), while from approximately 16 GHz the values of the phase propagation constant increase, whereas the slope of the curve decreases, thus giving rise to a narrow stopband region between 17.85 GHz and 17.96 GHz. At the end of the stopband region this second branch couples with the first branch of the perturbed TM_0 mode giving rise to the proper leaky wave described above. Due to the presence of this second real proper branch, the complete bandgap region for propagation along the x-direction in the case of PEC symmetry is very narrow (between 17.85 GHz and 17.96 GHz); even below 16 GHz, when the phase constant is almost superimposed to the light line, this second branch is expected to be weakly excited by finite sources.

At lower frequencies, a dominant TM_0 improper (forward) leaky mode (black dashed curves in Fig. 5(a)) is present. The normalized phase and attenuation constants of this improper leaky mode as a function of frequency are shown with more details in Fig. 6. The relevant fundamental, i.e., $(m,n)=(0,0)$, improper leaky Floquet harmonic, whose attenuation constant is indicated in Figs. 5(b) and 6 as black and gray dashed lines, respectively, lies in the fast-wave region $(|\beta_x/k_0|<1)$, indicated as a shadowed gray region in Fig. 5(a), and, hence, is physical below 7.6 GHz. In particular, when observing along the $+x$-direction $(\alpha_x>0)$, it is physical when $0<\beta_x/k_0<1$, and vice versa, when observing along the $-x$-direction $(\alpha_x<0)$, it is physical when $-1<\beta_x/k_0<0$. In both cases $\beta_{x,0}\alpha_x>0$, which confirms the improper (forward) nature of the physical leaky wave. Moreover, we can also observe that this kind of leaky wave is characterized by phase and group velocities that are

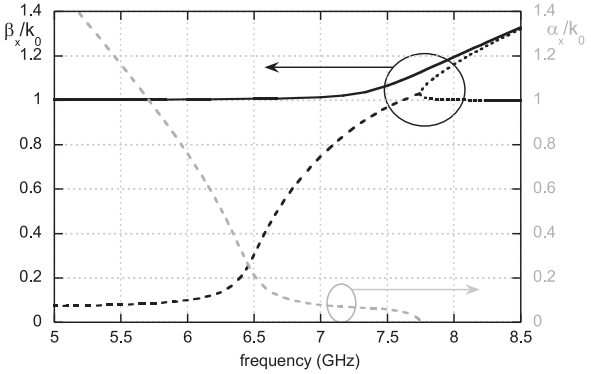

Fig. 6. Details at low frequencies of the phase (*black lines*, *left axis*) and attenuation (*gray line*, *right axis*) constants normalized by the free-space wavenumber as a function of frequency for the anti-symmetric TM modes propagating along the $+x$-direction. Legend: *phase constant*: solid lines – proper real; dotted lines – improper real; dashed lines – improper complex. *Attenuation constant*: dashed lines – improper complex.

in the same direction, i.e., the black dashed dispersion curves in the shadowed gray region in Fig. 5(a) have a negative (positive) slope when the phase constant is negative (positive). When the values of the attenuation constant (black and gray dashed lines in Figs. 5(b) and 6, respectively) are sufficiently low, directive leaky-wave radiation of the forward type is found, which can be considered for the design of 2D periodic leaky-wave antennas [26,27]. Above 7.6 GHz this improper leaky mode enters the spectral-gap region where the leaky mode is non-physical, since it lies within the slow-wave region $(|\beta_x/k_0|>1)$, even though its attenuation constant is different from zero, as shown in Fig. 6 [27]. By further increasing frequency, at 7.7 GHz a splitting point is observed, where the improper complex solution merges with a complex conjugate solution and the two solutions then split apart as two improper real branches (black dotted lines in Fig. 6) [27]. By increasing frequency from the splitting point, the higher improper real solution in Fig. 6 overlap with the first proper real branch of the perturbed TM_0 mode, while the lower improper real solution becomes tangent to the $\beta_x=\pm k_0$ curve and then it changes its spectral nature, with the $(m,n)=(0,0)$ Floquet harmonic being proper for frequencies above 8.25 GHz. The presence of such dominant TM_0 improper leaky mode at low frequencies is very unusual, since a grounded dielectric slab without periodic loading typically shows a TM leaky mode of the improper kind at higher frequencies below the cutoff of the TM_2 mode [32], and is the result of the strong periodic loading provided by the dogbone pairs at these frequencies.

We finally note that the metalayer analyzed in [8] (with the same dimensions as in this paper) shows a

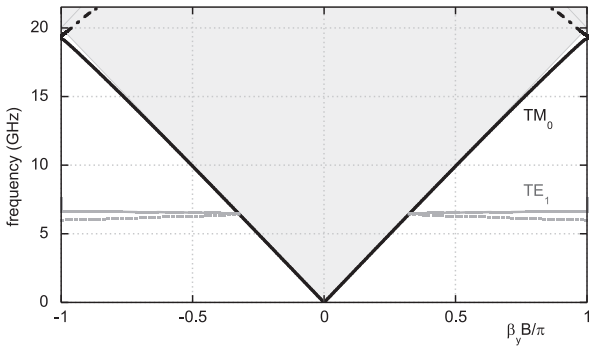

Fig. 7. Anti-symmetric modes propagating along the y-direction. Brillouin diagram (frequency versus $\beta_y B/\pi$). Legend: *phase constant*: solid lines – proper real; dashed-dotted lines – proper complex; dotted lines – improper real. The curves $\beta_y = \pm k_0$ are reported as light gray solid lines. The fast-wave region is indicated as a shadowed gray region.

transmission peak in proximity of the magnetic resonance (near 6.4 GHz), which is the frequency at which $\beta_x = \alpha_x$ for the LW in Fig. 6. At this frequency, a stack of metalayers supports backward propagation along z, as shown in Fig. 5 of [8].

3.2.2. *Modes propagating along the y-direction*

In Fig. 7 the fundamental $(m, n) = (0, 0)$ harmonic of the perturbed TE_1 mode propagating along the y-direction (with electric field polarized mainly along x) is shown in the Brillouin diagram. The cutoff frequency of the perturbed TE_1 mode (gray curves) is approximately 6.45 GHz, while that in the corresponding dielectric slab is equal to 69 GHz. The passband region of this physical mode is a very narrow one (between 6.45 GHz and 6.61 GHz), while below cutoff a non-physical real improper solution is present. Above 6.61 GHz a wide bandgap occurs for this mode, characterized by very high values of the attenuation constant, not reported here.

As concerns the TM_0 mode (black curves), it is weakly perturbed at low frequencies. Below 15 GHz the phase constant of the fundamental $(m, n) = (0, 0)$ harmonic (black solid curves in Fig. 7) is almost superimposed to the light line. At higher frequencies, a narrow stopband is present between 19.20 GHz and 19.46 GHz, followed by a very narrow second passband, between 19.46 GHz and 19.64 GHz, and a transition to a proper leaky wave (the $(m, n) = (0, -1)$ Floquet harmonic indicated as black dashed-dotted curve in Fig. 7, which is physical within the fast-wave region, i.e., the shadowed gray region in Fig. 7). Improper leaky waves with low attenuation constants are absent for propagation along the y-direction.

3.3. *Discussion*

In conclusion, the complete dispersion analysis of symmetric and anti-symmetric modes propagating along the principal x- and y-directions has shown that at low frequencies surface waves of both perturbed TE and TM polarizations are present below 19.96 GHz, which can modify the metamaterial performance of the arrayed pairs of metallic dogbones separated by a thin dielectric layer. In particular, a very narrow complete stopband is present between 17.85 GHz and 17.96 GHz for propagation along the x-direction, while surface-

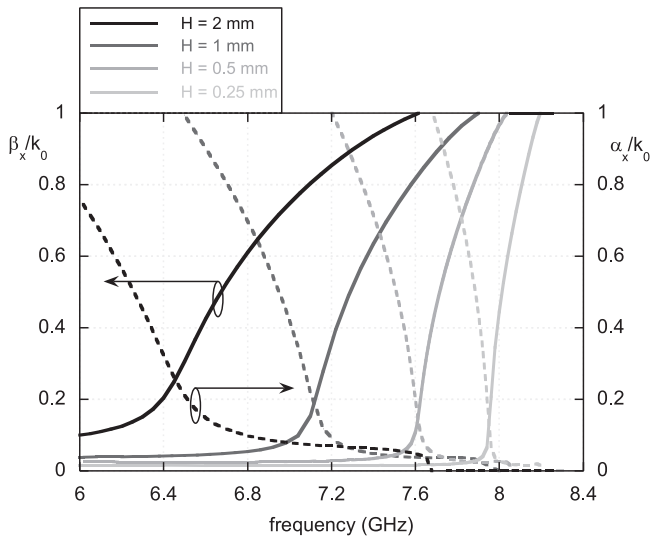

Fig. 8. Phase (*solid lines*, *left axis*) and attenuation (*dashed lines*, *right axis*) constants normalized by the free-space wavenumber as a function of frequency for the TM_0 improper leaky mode propagating along the x-direction, for different values of the slab thickness H.

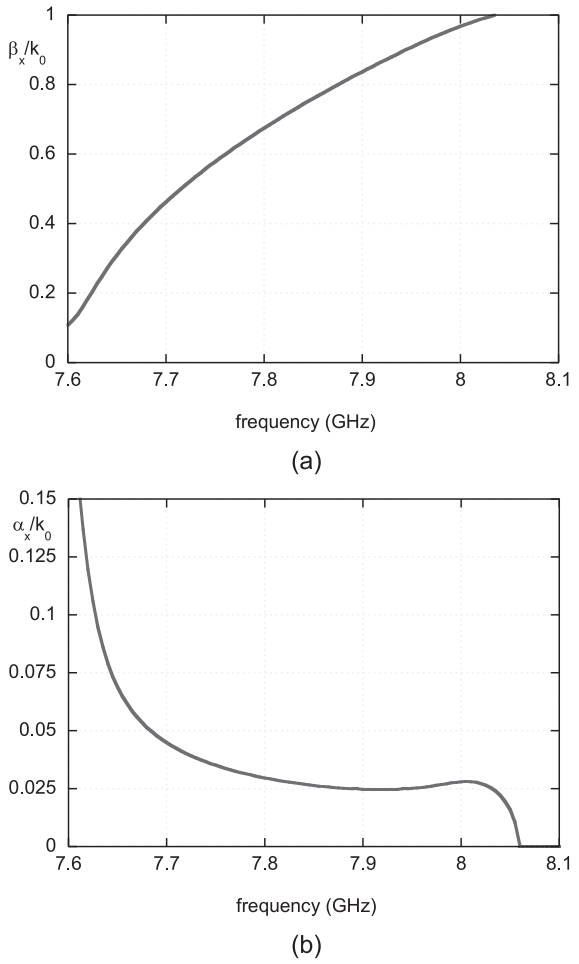

Fig. 9. Detail of the phase (a) and attenuation (b) constants normalized by the free-space wavenumber for the TM_0 improper leaky mode propagating along the x-direction, as a function of frequency for $H = 0.5$ mm.

and leaky-wave propagation is present at any frequency along y. Moreover, physical proper leaky-wave regimes are observed at higher frequencies (as usual for this kind of periodic structures [12,14]) above 18.2 GHz for propagation along the x-direction and above 19.64 GHz along the y-direction. Finally, a peculiar physical TM improper leaky-wave regime occurs for propagation along the x-direction below 7.7 GHz, where the magnetic (anti-symmetric) resonance and the effective negative refractive index of the tightly coupled dogbone pairs are experienced [1]. Also highly perturbed symmetric proper TM_1 and anti-symmetric proper TE_1 modes are present at low frequencies, which propagate along the x- and y-directions above 8.20 GHz and 6.45 GHz, respectively; no physical leaky-wave branches are observed in these cases.

In order to investigate the behavior of the fundamental TM_0 improper leaky wave and in view of a possible use of such thin metalayer as a periodic leaky-wave antenna at low frequency [26], a parametric analysis has been performed as a function of the dielectric thickness for this anti-symmetric leaky wave propagating along the x-direction. In Fig. 8, the phase constants in the region of physical leakage, i.e., $0 < \beta_x/k_0 < 1$, and the attenuation constants (solid and dashed lines, respectively) relevant to the in-plane TM_0 improper leaky mode traveling along the x-direction are shown for four different slab thicknesses ($H = 2$ mm, 1 mm, 0.5 mm, and 0.25 mm). By reducing the slab thickness, it is possible to obtain sufficiently low values of the normalized attenuation constant, which can give rise to directive radiation in a wide angle range as a function of frequency. In addition, the operating frequency of the leaky-wave antenna increases, while the leaky-wave antenna frequency range, which is encompassed between the frequencies at which $\beta_x = \alpha_x$ (radiation at broadside when both the propagation and attenuation constants are much smaller than k_0 [26]) and that at which $\beta_x = k_0$ (end-fire radiation [26]), narrows as the slab thickness reduces. In particular, in Fig. 9 a close-up of Fig. 8 for the case of $H = 0.5$ mm is shown. The frequencies at which $\beta_x = \alpha_x$ and $\beta_x = k_0$ are approximately 7.61 GHz and 8.04 GHz, respectively. Furthermore, the values of the attenuation constant normalized to the free-space wavenumber are well below 0.05 in a wide frequency range, thus permitting a directive beam scanning.

4. Conclusion

In this paper, we have presented a full-wave study of in-plane (i.e., transverse) natural modes propagating in the planar direction of a metamaterial layer (metalayer) formed by tightly coupled arrayed pairs of dogbone-shaped conductors. It is shown that the modal spectrum includes both perturbed TE and TM surface (bound) and proper and improper leaky modes. It is noticed that surface waves propagate at low frequencies with typical stopbands at higher frequencies (when the period is comparable with a half of guided wavelength). Most importantly, it is observed that the proposed structure is capable of supporting at low frequencies (i.e., periods much smaller than the free-space wavelength) a TM_0 improper leaky mode with very low attenuation constant, exhibiting an anti-symmetric current distribution, which has been associated in the previous studies [1,2,8] with artificial magnetism and with backward propagation along z when metalayers are stacked. The presence of such an improper leaky mode also implies that the

thin metalayer investigated here can be used at low frequencies as leaky-wave antenna operating at the forward radiation regime (if the leaky wave is properly excited).

References

[1] G. Donzelli, A. Vallecchi, F. Capolino, A. Schuchinsky, Metamaterial made of paired planar conductors: particle resonances, phenomena and properties, Metamaterials 3 (2009) 10–27.

[2] A. Valecchi, F. Capolino, Metamaterials based on pairs of tightly coupled scatterers, in: F. Capolino (Ed.), Theory and Phenomena of Metamaterials, CRC Press, Boca Raton, FL, 2009 (Chapter 19).

[3] J. Zhou, L. Zhang, G. Tuttle, T. Koschny, C.M. Soukoulis, Negative index materials using simple short wire pairs, Phys. Rev. B 73 (2006) 041101.

[4] J. Zhou, E.N. Economon, T. Koschny, C.M. Soukoulis, Unifying approach to left-handed material design, Opt. Lett. 31 (2006) 3620–3622.

[5] L. Markley, G.V. Eleftheriades, A negative-refractive-index metamaterial for incident plane waves of arbitrary polarization, Antennas Wireless Propagat. Lett. 6 (2007) 28–32.

[6] V. Podolskiy, A. Sarychev, V. Shalaev, Plasmon modes and negative refraction in metal nanowire composites, Opt. Express 11 (2003) 735–745.

[7] V.M. Shalaev, W. Cai, U.K. Chettiar, H.-K. Yuan, A.K. Sarychev, V.P. Drachev, A.V. Kildishev, Negative index of refraction in optical metamaterials, Opt. Lett. 30 (2005) 3356–3358.

[8] A. Vallecchi, F. Capolino, A Schuchinksy, 2-D isotropic effective negative refractive index metamaterial in planar technology, IEEE Microwave Wireless Comp. Lett. 19 (2009) 269–271.

[9] P. Baccarelli, F. Capolino, S. Paulotto, A.B. Yakovlev, Modal analysis of a metamaterial layer formed by arrayed pairs of planar conductors, in: Third International Congress on Advanced Electromagnetic Materials in Microwaves and Optics, London, UK, 30 August–4 September, 2009, 2009, pp. 761–763.

[10] A. Vallecchi, F. Capolino, Tightly coupled tripole conductor pairs as constituents for a planar 2D-isotropic negative refractive index metamaterial, Opt. Express 12 (2009) 15216–15227.

[11] H.L. Bertoni, L.H.S. Cheo, T. Tamir, Frequency-selective reflection and transmission by a periodic dielectric layer, IEEE Trans. Antennas Propagat. 37 (1989) 78–83.

[12] P. Baccarelli, S. Paulotto, C. Di Nallo, Full-wave analysis of bound and leaky modes propagating along 2D periodic printed structures with arbitrary metallisation in the unit cell, IET Microwave Antennas Propagat. 1 (2007) 217–225.

[13] G. Valerio, P. Baccarelli, P. Burghignoli, A. Galli, R. Rodriguez-Berral, F. Mesa, Analysis of periodic shielded microstrip lines excited by nonperiodic sources through the array scanning method, Radio Sci. 43 (2008), RS1009, doi:10.1029/2007RS003697.

[14] A.B. Yakovlev, O. Luukkonen, C.R. Simovski, S.A. Tretyakov, S. Paulotto, P. Baccarelli, G.W. Hanson, Analytical modeling of surface waves on high impedance surfaces, in: S. Zouhdi, A. Sihvola, A.P. Vinogradov (Eds.), Metamaterials and Plasmonics: Fundamentals, Modeling, Applications, Springer Science + Business Media B.V., 2009, pp. 239–254.

[15] C.R. Simovski, P.D. Maagt, I.V. Melchakova, High-impedance surfaces having stable resonance with respect to polarization and incidence angle, IEEE Trans. Antennas Propagat. 53 (2005) 908–914.

[16] A. Vallecchi, M. Albani, F. Capolino, Planar metamaterial transverse equivalent network and its application to low-profile antenna designs, in: European Conference on Antennas and Propagation (EUCAP), Berlin, Germany, 23–27 March, 2009, 2009, pp. 861–865.

[17] A. Vallecchi, F. Capolino, Thin high-impedance metamaterial substrate and its use in low profile antennas suitable for system integration, in: 59th Electronic Circuit and Technology Conference (ECTC), San Diego, CA, USA, 26–29 May, 2009, 2009, pp. 777–783.

[18] A. Vallecchi, F. Capolino, J. De Luis, F. De Flaviis, A low profile folded dipole antenna on a reactive high impedance substrate, in: International Conference on Electromagnetics in Advanced Applications (ICEAA), Turin, Italy, 14–18 September, 2009, 2009, pp. 1062–1065.

[19] F. Capolino, D.R. Jackson, D.R. Wilton, Field representations in periodic artificial materials excited by a source, in: F. Capolino (Ed.), Theory and Phenomena of Metamaterials, CRC Press, Boca Raton, FL, 2009, pp. 1–26.

[20] F. Capolino, D.R. Jackson, D.R. Wilton, Fundamental properties of the field at the interface between air and a periodic artificial material excited by a line source, IEEE Trans. Antennas Propagat. 53 (2005) 91–99.

[21] F. Capolino, D.R. Jackson, D.R. Wilton, L.B. Felsen, Comparison of methods for calculating the field excited by a dipole near a 2-D periodic material, IEEE Trans. Antennas Propagat. 55 (2007) 1644–1655.

[22] T. Tamir, A.A. Oliner, Guided complex waves—Part I. Fields at an interface, Proc. Inst. Elec. Eng. (Lond.) 110 (1963) 310–324.

[23] T. Tamir, A.A. Oliner, Guided complex waves—Part II. Relation to radiation patterns, Proc. Inst. Elec. Eng. (Lond.) 110 (1963) 325–334.

[24] T. Tamir, A.A. Oliner, The spectrum of electromagnetic waves guided by a plasma layer, Proc. IEEE 51 (1963) 317–332.

[25] A. Hessel, General characteristics of traveling wave antennas, in: R.E. Collin, F.J. Zucker (Eds.), Antenna Theory, McGraw-Hill, New York, NY, 1969, pp. 151–258.

[26] A.A. Oliner, D.R. Jackson, Leaky-wave antennas, in: J.L. Volakis (Ed.), Modern Antenna Handbook, McGraw-Hill, New York, 2007, ch. 11.

[27] D.R. Jackson, A.A. Oliner, Leaky-wave antennas, in: J.L. Volakis (Ed.), Antenna Engineering Handbook, John Wiley & Sons, Inc., New York, 2008, pp. 325–367.

[28] D. Pissoort, F. Olyslager, Study of eigenmodes in periodic waveguides using the Lorentz reciprocity theorem, IEEE Trans. Microwave Theory Tech. 52 (2004) 542–553.

[29] A.D. Yaghjian, Bidirectionality of reciprocal, lossy or lossless, uniform or periodic waveguides, IEEE Microwave Wireless Comp. Lett. 17 (2007) 480–482.

[30] G.W. Hanson, A.B. Yakovlev, Investigation of mode interaction on planar dielectric waveguides with loss and gain, Radio Sci. 34 (1999) 1349–1359.

[31] P. Baccarelli, S. Paulotto, D.R. Jackson, A.A. Oliner, A new Brillouin dispersion diagram for 1-D periodic printed structures, IEEE Trans. Microwave Theory Tech. 55 (2007) 1484–1495.

[32] D.R. Jackson, A.A. Oliner, A leaky-wave analysis of the high-gain printed antenna configuration, IEEE Trans. Antennas Propagat. 36 (1988) 905–910.